IEEE Access
Multidisciplinary | Rapid Review | Open Access Journal

Received 11 June 2025, accepted 23 June 2025, date of publication 30 June 2025, date of current version 9 July 2025.

Digital Object Identifier 10.1109/ACCESS.2025.3584560

RESEARCH ARTICLE

Optimization Method of Wind Turbine Locations in Complex Terrain Areas Using a Combination of Simulation and Analytical Models

DINH VAN THIN[1], LE QUANG SANG[2,3], AND NGUYEN HUU DUC[4], (Member, IEEE)

[1]Faculty of New Energy, Electric Power University, Hanoi 11917, Vietnam
[2]Faculty of Energy Engineering, School of Electrical and Electronics Engineering, Hanoi University of Industry, Hanoi 11915, Vietnam
[3]Institute of Science and Technology of Energy and Environment, Vietnam Academy of Science and Technology, Hanoi 100072, Vietnam
[4]Faculty of Control and Automation, Electric Power University, Hanoi 11917, Vietnam

Corresponding author: Nguyen Huu Duc (ducnh@epu.edu.vn)

This study was supported by the Master, PhD Scholarship Programme of Vingroup Innovation Foundation (VINIF): ''Dinh Van Thin was funded by the Master, PhD Scholarship Programme of Vingroup Innovation Foundation (VINIF), code VINIF.2024.TS.090''.

ABSTRACT Once an area has been identified for a wind farm, the annual energy production of the farm is the most important quantity to obtain high exploitation efficiency. This quantity depends mainly on factors such as wind resource characteristics, type, number and arrangement of turbines. For areas with complex terrain, wind resource characteristics depend largely on terrain features, so the selection of turbine installation locations is very important. Because when the turbines operate, they will cause a wake effect that increases the turbulence of the flow behind. Therefore, it is necessary to find the optimal distance between turbines so that the annual energy production reaches the maximum value. This study presents a method to determine the optimal turbine locations when considering the correlation between wake loss and turbine space in the case of mountainous terrain. Firstly, a computational fluid dynamics model combined with a geographic information system are used to determine the 3-dimensional wind characteristics at specific locations. Secondly, a Jensen model is used to consider the wake effect according to the distance between turbines. Then, the the annual energy production values are determined through the analytical model. In addition, a comprehensive assessment of levelized cost of energy is also provided to confirm the practicality of implementing the optimization model. Finally, the optimal location configuration of the turbines is proposed. This method was tested and compared with a farm with sufficient data to assess reliability and then applied to an area in Ninh Thuan, Viet Nam. The results showed that the the annual energy production obtained from this farm can be up to 252.3 GWh (30 turbines) compared to 99.9 GWh (10 turbines), which is 2.5 times larger.

INDEX TERMS Annual energy production, CFD-GIS, levelized cost of energy, wake effect, wind energy, wind farm, wind turbine placement optimization.

NOMENCLATURE

ACRONYMS

3D	Three-dimentional.
BEM	Blade element momentum.
CBWES	Columbia Basin Wind Energy Study.
CFD	Computational Fluid Dynamics.
GIS	Geographic information system.
LES	Large-eddy simulation.
RANS	Reynolds-averaged Navier-Stokes.
WFR	Weather research and forecasting.

VARIABLES AND OPERATORS

A	Cross-section area.
a	Axial induction factor.
AEP	Annual energy production.

The associate editor coordinating the review of this manuscript and approving it for publication was Akshay Kumar Saha.

C_P	Power factor.
d	Distance.
D_{rotor}	Rotor diameter.
f (U)	Weibull distribution function.
i, j	Index of a turbine.
K	Eddy viscosity.
l	Length.
m	Number of wind speed intervals.
n	Number of turbine rows.
LCOE	Levelized costs of energy.
P	Power.
p	Pressure.
P_e	Output electrical power.
r_{cw}	Rate of change of wind speed with terrain slope.
S	Scale parameter.
T	Force.
U	Wind speed.
VD	Velocity deficit.
W	Width parameter.
WL	Wake loss.

I. INTRODUCTION

Wind energy is chosen as an important alternative energy source for many countries to cope with climate change. To improve the efficiency of wind farms, it is necessary to consider factors such as wind resource characteristics and turbine technology used. Wind resource characteristics depend on many factors including terrain and climate specific to each turbine installation location. Accurate assessment of wind resource characteristics is a difficult problem and requires a lot of resources and budget [1]. After the wind resource characteristics are determined, the selection of appropriate turbine technology also needs to be carried out [2].

To determine the characteristics of the wind resource, some experimental measurement systems can be used. However, the cost of these measurement systems is quite large and it is impossible to conduct measurements at all different locations in the wind farm planning area. In addition, statistical models and artificial intelligence models based on experimental measurement data are also commonly used [3], [4], [5], [6], [7], [8]. However, these models also require providing sufficient experimental data to ensure the reliability of the prediction results. Obviously, state-of-the-art artificial intelligence algorithms still have many limitations in solving the problem of optimizing turbine installation locations [9]. In practice, simulation methods combined with a small amount of experimental data are usually used to verify even in flat or complex terrain conditions [10], [11]. Those methods significantly reduce the costs and difficulties in measuring experimental data. In general, to be able to simulate the wind resource for wind farms, it is necessary to approach the direction of gradually reducing the scale. Firstly, the global convection models need to be surveyed at a scale of about 10^7m. Next, the regional meteorological models are also considered based on a scale of about 10^5m. Then, the local meteorological models and the wind farm construction area are surveyed with a scale of about 10^2m. Even the meteorological characteristics at each location where the turbine is expected to be installed also need to be determined in complex terrain conditions [12]. Normally, the meteorological models are built based on reanalysis data obtained from satellite images using the weather research and forecasting (WRF) models. However, the WRF models can only provide preliminary data on the weather of each area and locality, but does not include other detailed factors such as the influence of terrain at each construction site and the operation of the turbines [13]. Therefore, the WRF models need to be combined with other analytical models to obtain more reliable results.

According to [12], the researchers compared several models to simulate the surface wind resource characteristics at Alaiz mountain in the North of Spain. The large-eddy simulation (LES) model and the Reynolds-averaged Navier-Stokes (RANS) model were used in combination with WRF. Both models provide high reliability for areas with complex terrain. However, the LES model has higher reliability but also requires a high computer system and more analysis time [12], [14]. For wind farm scale, it was reported that improper placement of wind turbines can reduce the total output capacity by up to 40% due to wake losses. According to [15], the research group combined the LES model and the WRF model with spatial resolution from 12.15km to 0.03km. Then, the results obtained from the simulation were compared with the experimental results referenced from the US Department of Energy [16]. The paper showed a very good agreement between the simulation and the experiment of the probability density functions and turbulence characteristics of the flow around the area with coordinates (45.9551 °N, −118.6877 °W). In addition, a study on the sensitivity of different WRF-based atmospheric boundary layer analysis models in this area is also presented in the [17]. Similarly, a study combining simulation and experiment for wind turbines in the coastal area of Thailand is also found in the publication of Lattawan et al. [18]. The published results showed that the effects of wake and terrain can reduce the output capacity by up to about 10%. In addition, studies using the RANS model to determine the farm configuration, then combined with economic models to evaluate the investment efficiency of wind power projects have also been conducted in many countries. These reports showed that optimizing the location and type of wind turbines can reduce the levelized costs of energy (LCOE) by hundreds of USD per 1 MWh and the farm area can be reduced by up to 30%. This clearly demonstrates the great benefits of the problem of optimizing the location and type of turbines for investors and governments [19], [20], [21], [22], [23], [24].

When turbines operate, wake effects will appear. These effects not only reduce the total output power but also increase the load on the rotor of the turbines, it can break the blades in case of extreme weather. Wake effects can be divided into near wake and far wake, the distance is greater than 4 times the rotor diameter. Near wake depends largely on

the turbine blade configuration, while far wake depends largely on the surrounding terrain. In the case of flat terrain, the wind velocity distribution farther from the first turbine tends to be symmetrical with respect to height like Gaussian distribution [25]. Some commonly used theoretical models describing wake effects are Jensen, Larsen, Fuga, Lissaman and Frandsen. Among them, Jensen's wake model is more commonly used, meeting the accuracy for both onshore and offshore wind farms [26], [27], [28]. However, in cases where the terrain has large changes in slope, such as the sea adjacent to the mountains or the valley surrounded by mountains, these analytical models often cannot cover the wind changes. Therefore, it is necessary to combine with other 3D visualization methods such as LES, RANS or WRF [29], [30], [31], [32].

Obviously, the LES or RANS methods combined with the WRF model are very suitable for determining the wind resource characteristics of farms with complex terrain. However, these combined methods also require very high computer configuration and long calculation time, which can last for weeks for large-scale wind farms. To solve the limitations of computer resources or calculation time, geographic information system models are increasingly used. The GIS models will provide information about the terrain and weather patterns of any areas. Recently, the outstanding features of GIS are being exploited in the latest studies on optimal design calculation for wind farms [33]. This information will then be fed into RANS-CFD models to analyze the flow processes more thoroughly through conservation equations [34], [35], [36]. The LES solver has high accuracy in simulating aerodynamic processes in time series, including calculations of the effects of weather factors, the interactions of turbine with the atmosphere. The RANS solver is often applied to aerodynamic problems in a static state, the effects of the surrounding weather model are not considered. However, LES requires higher computer configuration and calculation time than RANS. This study focuses on the interactions between the steady state flow and the turbines in one main direction. In the case of analysis with static flow, the accuracy of RANS and LES is not significantly different, but RANS is more efficient in terms of calculation time [37], [38], [39]. Therefore, the RANS solver was chosen instead of the LES solver.

In this study, a new method will be proposed. Firstly, GIS is used to determine the 3D topographic features of a wind farm. Then, RANS-CFD model will be implemented to determine the steady-state wind resource characteristics for each location in the area. Finally, theoretical models such as BEM, Jensen's wake will be used to calculate the AEP, WL and LCOE values according to the parameters and configurations of of the turbines in the wind farm. From there, the optimal turbine location configuration for the wind farm will be determined based on comprehensive considerations. This method was firstly verified in the mountainous area around the coordinates (45.9551 °N, −118.6877 °W). Then, it was applied to determine the optimal installation configuration of Enercon E103 turbines for a wind farm around the coordinates (11.4642 °N, 109.0049 °E) in Ninh Thuan province, Viet Nam. Finally, the location configuration with the maximum the annual energy production (AEP) value was determined for this area. The obtained results show that the AEP value can reach 247.7 GWh, about 2.5 times higher than the existing configuration. Meanwhile, the LCOE value has a slight difference, about 81.2 $/MWh compared to 67.1 $/MWh. According to the National Power Development Plan for the period 2021-2030, with a vision to 2050 [40], Viet Nam will prioritize the maximum development of wind power sources. By 2030, the total onshore and nearshore wind power capacity will reach 26.1 GW – 38.0 GW. The total offshore wind power capacity serving domestic electricity demand is about 6.0 GW - 17.0 GW, expected to operate in the 2030-2035 period. The orientation to 2050 is to reach 113.0 GW – 139.1 GW. The estimated offshore wind power capacity for new energy production is about 15.0 GW in 2035 and about 240.0 GW in 2050. To achieve these goals, wind farm design studies to optimize exploitation and investment efficiency need to be given special attention. In fact, Viet Nam has a mostly mountainous terrain, so in order to build the most efficient wind farms, it is necessary to solve the problem of wind resource distribution according to complex terrain. Then, the type of turbine and the optimal location configuration need to be calculated according to the planned area. This is also a big challenge that the government and investors are facing.

This paper is divided into four main parts: The first part introduces some methods currently used to evaluate the wind resource, thereby presenting some difficulties that need to be solved. Then, a new method to solve the problem is proposed; the second part presents the components and structure of the new method, including the contents related to BEM theory, AEP and Weibull function, Jensen's wake, GIS and CFD; the third Part presents the obtained results and comments when verifying with an area with some experimental parameters and when applying to a mountainous area adjacent to the sea in Ninh Thuan province, Viet Nam; The last part briefly presents some conclusions from the obtained results and future research orientation.

Three key contributions of this paper are as follows:

- A comprehensive analytical model combining the superior features of modern tools such as GIS, CFD and theoretical models to optimize calculations for onshore wind farms was developed.
- The optimal configuration for the wind farm to effectively exploit wind energy on the same land area was proposed. This configuration helps the wind farm achieve the largest AEP value along with reasonable WL and LCOE values.
- The reliable scientific method was presented to help managers and investors to refer to plan the most effective wind power projects. Thus, it make a contribution to enhancing the role of wind power in the roadmap to achieve the net-zero emission target of Viet Nam by 2050.

II. WIND TURBINE PLACEMENT OPTIMIZATION METHOD

A. BEM THEORY

The theoretical model for determining the power of wind turbines was proposed by Betz and Glauert in the 1930s. Initially, the characteristics of the turbine were determined based on the moment theory and the blade element theory. Later, these two theories were combined into the BEM theory. Currently, the BEM theory is widely used in the aerodynamic design and performance analysis of wind turbine rotors. This theory assumes that the air flow will move through a control volume, which is limited by cylindrical surfaces. The turbine is represented by a rectangular actuator disc as shown in Fig. 1. The air flow moving through the control volume is assumed to be incompressible, uniform in density and steady [2], [41], [42].

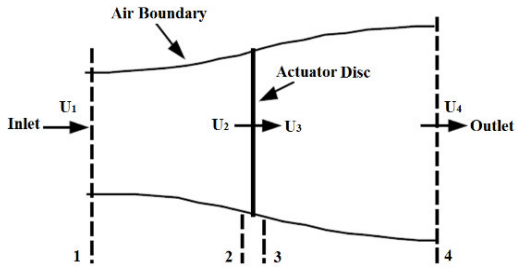

FIGURE 1. One-dimensional momentum theory model.

This theory assumes that the number of turbine blades is infinite, the force acts uniformly on the entire actuator disc, and no vortices are created behind the turbine when it rotates. When considering the above system as closed and using the law of momentum conservation, the force acting on this turbine can be determined as in Eq. (1):

$$T = U_1 (\rho A_1 U_1) - U_4 (\rho A_4 U_4) \tag{1}$$

In which: ρ is the air density, kg/m^3; A_1 and A_2 are the cross-sectional areas at inlet 1 and outlet 4, m^2; U_1 and U_4 are the wind speeds at inlet 1 and outlet 4, m/s.

Under steady flow conditions, the law of mass conservation allows determining the flow rate as Eq. (2):

$$\dot{m} = \rho A_1 U_1 = \rho A_4 U_4 \tag{2}$$

Substituting Eq. (2) into Eq. (1), we have:

$$T = \dot{m} (U_1 - U_4) \tag{3}$$

Bernoulli's law for the fluid flow in front of the turbine:

$$p_1 + \frac{1}{2}\rho U_1^2 = p_2 + \frac{1}{2}\rho U_2^2 \tag{4}$$

Bernoulli's law for the fluid flow behind the turbine:

$$p_3 + \frac{1}{2}\rho U_3^2 = p_4 + \frac{1}{2}\rho U_4^2 \tag{5}$$

The pressure at the inlet and outlet is equal to the environmental pressure, so $p_1 = p_4$. The flow velocity before the turbine and after the turbine is equal, $U_2 = U_3$. Then, the force acting on one side of the turbine is determined as follows:

$$T = A_2 (p_2 - p_3) = \frac{1}{2}\rho A_2 \left(U_1^2 - U_4^2\right) \tag{6}$$

Combining Eq. (3) and Eq. (6), we have:

$$U_2 = \frac{U_1 + U_4}{2} \tag{7}$$

The value of the axial induction factor (a) along the horizontal axis of the incoming flow for the rotor is determined as follows:

$$a = \frac{U_1 - U_2}{U_1} \tag{8}$$

From here, the power generated by the turbine is determined as follows:

$$P = TU_2 = \frac{1}{2}\rho A_2 \left(U_1^2 - U_4^2\right) U_2 = \frac{1}{2}\rho A_2 U_1^3 4a (1-a)^2 \tag{9}$$

Let C_P be the power factor, which is the ratio of the power produced by the turbine to the power of the inlet freestream:

$$C_P = \frac{P}{\frac{1}{2}\rho A_2 U_1^3} = 4a (1-a)^2 \tag{10}$$

From Eq. (10), we can find the maximum value of C_P is 16/27, at a = 1/3. This means that the best turbine design will have the flow velocity at the front surface being 2/3 of the incoming flow velocity and the highest wind energy extraction efficiency that can be achieved is only 59.26%. The power generated by the turbine will be converted into output electrical power through the mechanical systems, the mechanical conversion efficiency is denoted by η_{mech}. From here, the output electrical power of the turbine can be determined as follows:

$$P_e = \frac{1}{2}\rho A_2 U_1^3 C_P \eta_{mech} \tag{11}$$

The annual electricity production of the turbines can also be determined according to Eq. (12) [18], [43]:

$$AEP = 8760 \sum_{i=1}^{n} \sum_{j=1}^{m} \left(Pe_j^i f_j^i\right) \tag{12}$$

where: AEP is the annual electricity production, kWh; n is the number of turbine rows; m is the number of wind speed intervals; Pe_j^i is the turbine's output power for wind speed interval j at row i, kW; f_j^i is the Weibull distribution function value of wind speed interval j at row i.

Weibull distribution function is expressed as in the Eq. (13):

$$f(U) = \left(\frac{W}{S}\right)\left(\frac{U}{S}\right)^{W-1} Exp\left(-\left(\frac{U}{S}\right)^{W}\right) \tag{13}$$

With W and S are the width and scale parameters of the wind speed distribution, respectively.

The parameter that causes the largest error for AEP is the wind speed frequency. Therefore, the error of AEP will be determined by the error propagation method through the Weibull function as follows:

$$\Delta AEP = 8760 \sum_{i=1}^{n} \sum_{j=1}^{m} \left(Pe_j^i \Delta f_j^i \right) \tag{14}$$

With:

$$\Delta f_j^i = \frac{\mathrm{W}}{S^2} Exp\left(-\left(\frac{U}{S} \right)^{\mathrm{W}} \right) \left[(\mathrm{W}-1) \left(\frac{U}{S} \right)^{\mathrm{W}-2} - \mathrm{W} \left(\frac{U}{S} \right)^{2(\mathrm{W}-1)} \right] \Delta U_j^i \tag{15}$$

where: ΔAEP is the absolute error of AEP, kWh/year; Δf_j^i is the absolute error of wind speed frequency at location (i,j); ΔU_j^i is the absolute error of wind speed when arriving at the turbine at location (i,j), m/s.

The wake loss can be determined as in Eq. (16):

$$\mathrm{WL} = \left(1 - \frac{AEP}{AEP_{no-wake}} \right) \times 100\% \tag{16}$$

where: WL is the wake loss, %; AEP and $AEP_{no-wake}$ are the annual electricity production with and without wake effects, respectively.

B. WAKE EFFECTS

Wake models are used to determine the effect on the output power of turbines when their spacing is different. As the blades of the first turbine rotate, wake vortices are created behind. These vortices gradually expand with the distance behind the turbine. The wake vortices cause an increase in turbulence intensity and a decrease in the velocity of the airflow to the following turbines [44], [45]. Two main components are velocity deficit and turbulence intensity of the flow behind the turbines need to be considered. The wind speeds at these different locations are affected by wake due to both the forward turbines and the terrain slope. Each area has a different terrain slope and the rate of change of wind speed with terrain slope (r_{cw}) needs to be determined by CFD. The wind speed at the rear turbine at a distance will be multiplied by r_{cw} as shown in Eq. (17) [25], [26]:

$$U_d = r_{cw} U_1 \left[1 - \frac{a}{\alpha_d \frac{d}{D_{rotor}}} \right] \tag{17}$$

Then, the velocity deficit (VD) at point d behind the rotor is determined as in Eq. (18):

$$VD = \left(1 - \frac{U_d}{U_1} \right) 100\% = \left(\frac{a}{\alpha_d \frac{d}{D_{rotor}}} \right) 100\% \tag{18}$$

where: U_1 is the wind speed to the first turbine, m/s; U_d is the wind speed behind the turbine at position Z, m/s; D_{rotor} is the rotor diameter, m; a is an axial induction factor of the turbine; α_d is a decay coefficient, $\alpha_d = 0.075$ for onshore wind farms [41].

Obviously, the value of U_d can be determined through some approximate assumptions for the terrain type and turbine type. However, in this study, the exact values of U_d will be determined by a modern method based on a combined GIS model and CFD model.

C. GIS AND CFD MODELS

GIS model provides geographic data and maps of the terrain of areas with high accuracy based on satellite images. Therefore, this model is essential to provide 3D maps of complex objects such as urban or mountainous areas. In recent years, they have been widely used in studies on site selection for wind farms [46], [47], [48], [49]. In this study, BlenderGIS will be used to provide 3D maps of wind farms. BlenderGIS is an open source code with full features and easy to use for researchers who are not specialized in the field of digital maps [34], [50].

CFD is a model that simulates the motion, interaction, heat transfer or reaction of fluids based on conservation equations such as mass conservation, momentum conservation and energy conservation. This model is often used in fields such as aviation, aerospace and energy systems. The conservation equations that govern fluid processes are commonly known as the Navier-Stokes equations and they are often implemented in the form of partial differential equations. For example, mass conservation is often expressed through the continuity equation; momentum conservation is expressed through Newton's second law; energy conservation is expressed through the first law of thermodynamics as expressed in Eqs. (19)-(21) [51], [52].

Continuity equation:

$$\frac{\partial \rho}{\partial t} + \nabla \left(\rho \vec{U} \right) = 0 \tag{19}$$

Newton's second law equation:

$$\frac{\partial \vec{U}}{\partial t} + \vec{U} \nabla \vec{U} = -\frac{\nabla p}{\rho} + \nu \nabla^2 \vec{U} + \vec{f_b} \tag{20}$$

First law of thermodynamics equation:

$$\frac{\partial (\rho h_{tot})}{\partial t} - \frac{\partial p}{\partial t} + \nabla \left(\rho \vec{U} h_{tot} \right) = \nabla (\lambda \nabla T) + \nabla \left(\vec{U} \tau \right) + S_E \tag{21}$$

where: U is velocity, m/s; p is the static pressure of the fluid, Pa; ν is the viscosity of the fluid; f_b is gravity, N; h_{tot} is total enthalpy; λ is conductivity; T is temperature, K; τ is viscous stresses; S_E is the additional energy source from outside the system; t is time, s.

The conservation equations from (19) to (21) are often solved by the RANS technique. In the field of wind energy, the flow of air is often turbulent. Therefore, turbulent flow models are often used to determine more accurately the values of wind speed and pressure at each point in space. In which, the $k - \varepsilon$ turbulent flow model is often used and has been verified by many previous research groups [32], [52]. The

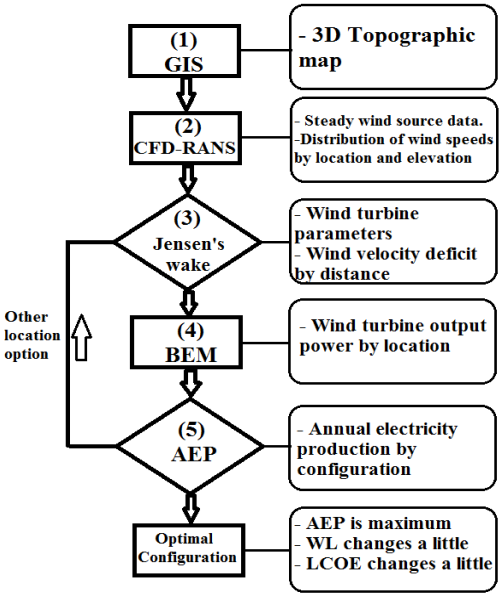

FIGURE 2. The procedure of determining the optimal turbine installation locations.

turbulent flow equation system in this model is represented as in Eq. (22):

$$\begin{cases} \dfrac{\partial k}{\partial t} + U_j \dfrac{\partial k}{\partial x_j} - \dfrac{\partial}{\partial x_i}\left(\dfrac{K}{\sigma_k}\dfrac{\partial k}{\partial x_i}\right) = P - \varepsilon + B \\ \dfrac{\partial \varepsilon}{\partial t} + U_j \dfrac{\partial \varepsilon}{\partial x_j} - \dfrac{\partial}{\partial x_i}\left(\dfrac{K}{\sigma_\varepsilon}\dfrac{\partial k}{\partial x_i}\right) = \dfrac{\varepsilon}{k}\left(C_{\varepsilon 1}P - C_{\varepsilon 2}\varepsilon + C_{\varepsilon 3}B\right) \end{cases} \tag{22}$$

where: k is turbulent kinetic energy;ε is turbulent eddy dissipation; x_i are the longitudinal, lateral and vertical directions, $x_1 = x, x_2 = y, x_3 = z$; K is the eddy viscosity; $\sigma_k = 1.0$, $\sigma_\varepsilon = 1.3$ are the Prandtl numbers; P is the production of k due to shear; B is the buoyancy term; $C_{\varepsilon 1} = 1.21, C_{\varepsilon 2} = 1.92$, $C_{\varepsilon 3} = 1.0$ are the model coefficients.

By solving the system of Eq. (22) and comparing with experiment, the value of the eddy viscosity K and its length l are determined as in Eq. (23) for the flow of air in the surface layer [53], [54], [55]:

$$\begin{cases} K = C_\mu \dfrac{k^2}{\varepsilon} \\ l = C_\mu^{3/4} \dfrac{k^{3/2}}{\varepsilon} \end{cases} \tag{23}$$

D. THE OPTIMIZATION MODEL STRUCTURE

Through the synthesis, analysis and evaluation of the above contents. This paper has proposed a method of combining simulation and analytical models to determine the most optimal installation locations in consideration of wake effects and distance factors to obtain the highest AEP value. The models used in this report are modern and highly reliable such as GIS, CFD-RANS, Jensen's wake and BEM. The specific steps of this method are shown in Fig. 2.

In the first step, a GIS tool will be used to create a 3D terrain model of the area of interest. Infrastructure and terrain elevation data will be created based on satellite image data with spatial resolution of meters. Then, this terrain model will be analyzed by CFD method with RANS solver to build wind speed distribution for each location and elevation in the farm. In the third step, wind velocity deficits of the existing and assumed configurations will be calculated by Jensen's wake theory based on turbine type and wind speed distribution at each point. BEM theory will determine the output power values of the turbines according to wind velocity deficits at each location in step 4. The AEP values of the whole farm will be determined based on the results of step 4 combined with the Weibull distribution function corresponding to each assumed configuration. From there, the configuration with the largest AEP value will be determined. For a comprehensive evaluation, WL and LCOE comparisons are performed to ensure the feasibility of the selected optimal configuration.

III. RESULTS AND DISCUSSION

The steps presented in the method for determining the optimal location of wind turbines in an area as shown in Fig. 2 will be used to calculate for a wind farm in Ninh Thuan province, Viet Nam. Previously, this method will be applied to a farm located around the location with coordinates (45.9551°N, −118.6877°W) for a reliability survey.

A. EVALUATION OF THE RELIABILITY

According to the [16], Pacific Northwest National Laboratory conducted wind resource characterization measurements from November 16, 2010 to March 21, 2012 in northeastern Oregon. This project, Columbia Basin Wind Energy Study (CBWES), provided experimental data on wind speed and wind direction in this complex terrain area, according to the height of the atmospheric boundary layer. The measurements used propeller, vane and sonic anemometers mounted on a 62 m tower and a wind profiler radar to collect and process the data. The coordinate location of this tower is (45.9551°N, −118.6877°W) as marked in Fig. 3. Currently, this area has been installed and operated with 454 Vestas V47 wind turbines. The brief technical specifications of the turbines are shown in Table 1. The wind resource and terrain data of this area are very complete, so this area was chosen to evaluate the reliability of the method proposed in this paper.

According to the first step of the method as shown in Fig. 2, the 3D topography of the area around the coordinates (45.9551°N, −118.6877°W) is recorded through GIS data by BlenderGIS V3.4 software. The objects will be determined according to the height above ground surface level as shown in Fig. 3. Then, the topography of this area will be imported into Ansys CFX software, V2024 student, to continue to build boundary conditions for the problem of determining wind source characteristics.

Fig. 4 shows the meshing model of the area around the coordinates (45.9551°N, −118.6877°W). The ground around the area will be the bottom surface of the model with a length

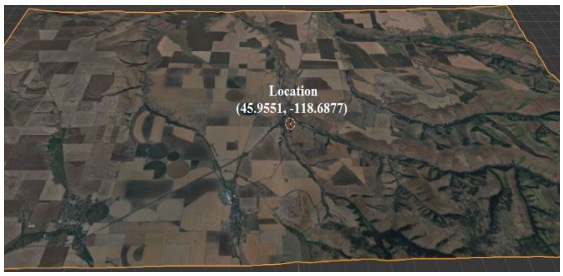

FIGURE 3. Topography of the area was built in BlenderGIS.

TABLE 1. Some main parameters of the Vestas V47 turbine [56], [57].

Quantity	Value	Quantity	Value
Manufacturer	Vestas	Power control	Pitch
Model	V47/660	Cut-in wind speed	4.5 m/s
Rotor diameter	47 m	Rated wind speed	15 m/s
Number of blades	3	Cut-off wind speed	25 m/s
Tower hight	55 m	Rated power	660 kW

of 12000 m, a width of 8000 m, the space above has an altitude of 500 m compared to the lowest surface position. The largest mesh element size is 100 m, the first boundary layer has a distance from the ground of 10 m, the ratio between boundary layers is 1.2, the total number of boundary layers is 5. These parameters have been used in some previous similar publications [32], [58]. This model has a total of 994735 elements and 210697 nodes. Using a computer configuration with a core i7 processor and 128 Gb ram, the analysis run time is about 30 minutes for one model.

FIGURE 4. Meshing for the 3D topography.

To determine the boundary conditions for the model, wind resource data needs to be collected. In this study, the inlet wind speed and wind direction conditions are determined from WorldBank data [59] as shown in Fig. 5. The wind speed and wind direction at heights of 10 m, 50 m, 100 m, 150 m and 200 m will be determined by taking the average value within an area of 96000000 m^2 around the point with coordinates (45.9551°N, −118.6877°W).

The average values of wind speed at 5 different height locations are shown and fitted in Figure 6. This theoretical fitting function represents the relationship between the wind speed distribution with height for terrain surfaces with different

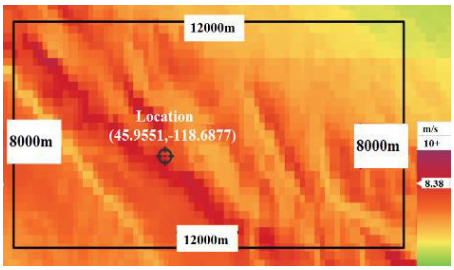

FIGURE 5. The area was used to calculate wind source characteristics [59].

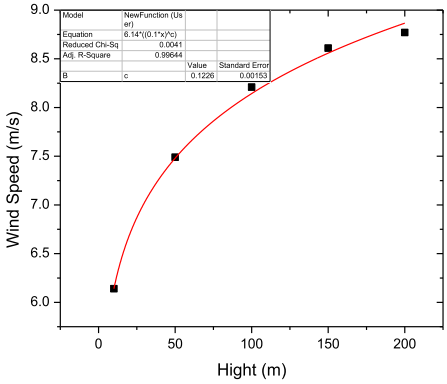

FIGURE 6. Mean wind speed distribution according to the height of the model.

characteristic roughness. In the case of flat terrain surfaces, the Hellmann exponent is 0.14. According to various publications, the value of this coefficient lies in the range from 0.1 to 0.3 [1] or in a wider range from 0.05 to 0.5 [60] depending on the specific terrain types and atmospheric stability. The theoretical fitting function obtained from Fig. 6 is shown in Eq. (24) with a Hellmann exponent of 0.12, which is used to establish the value of the mean wind speed with respect to height at the inlet plane of the analytical model:

$$WindSpeed = 6.14\left(\frac{h}{10}\right)^{0.12} \tag{24}$$

From Eq. (24), the mean wind speed at a height of 62 m is calculated to be 7.64 m/s, which is very close to the experimental measurement value of 7.7 m/s by the research team at the Pacific Northwest National Laboratory [16]. In this case, the deviation between the values obtained from the model and the experiment is only about 0.8%. This proves that the data source and the analytical model built in this study are highly reliable. Furthermore, according to the [61], the wind speed at an altitude of 80m in the coordinate area of (45.9551°N, −118.6877°W) has a value of about 7.5 m/s to 8.0m/s as shown in Fig. 7. This value is very consistent with the values obtained from Eq. (22). This further confirms the reliability of the wind speed distribution function according to altitude used in this research model.

The wind direction through this area was also determined from WorldBank data [59] and is shown in Fig. 8. From here, the main wind direction is determined to be at the

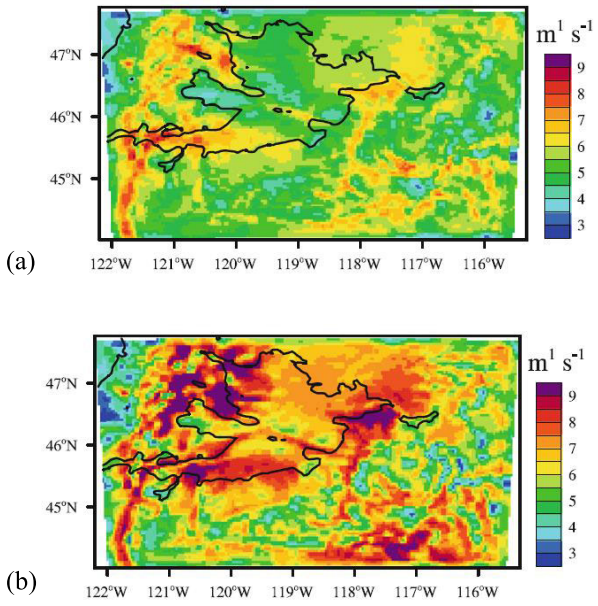

FIGURE 7. Average wind speed at 80m height: (a) Day, (b) Night [61].

angle between the west and south, accounting for about 60%. This wind direction is also consistent with the wind direction determined experimentally by the Pacific Northwest National Laboratory. This direction will be used to establish the incoming wind direction at the entrance plane in the analytical model.

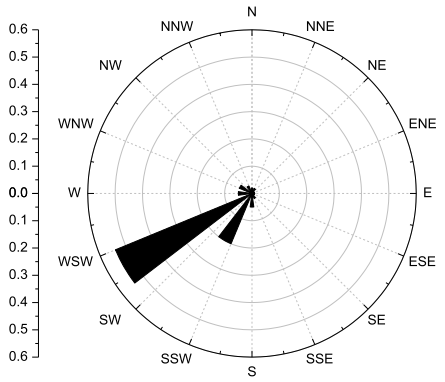

FIGURE 8. Incoming wind direction and wind speed ratios corresponding to the angles.

Based on the collected data, this simulation model continues to be set with boundary conditions as shown in Fig. 9. Accordingly, the west and south surfaces will be the incoming wind direction, the east and north surfaces will be the outgoing wind direction. The main wind direction will create an angle of 30° with the ox axis. The ground is set as a wall condition and the air surface above will be an open condition.

In addition to the parameters of wind speed and direction, the turbulence kinetic energy of the flow through this area is also a quantity that plays an important role in the accuracy of the model. According to the researched results of the group Laura et al. [62], the turbulence kinetic energy of the wind

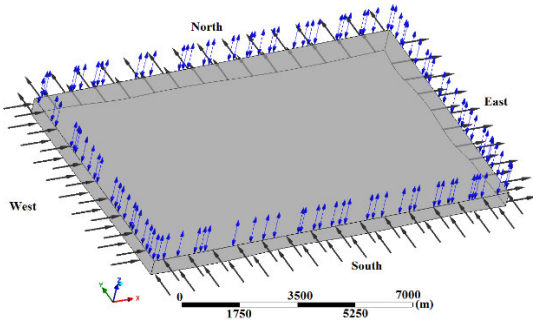

FIGURE 9. Setting boundary conditions for the 3D model.

flow in this area will have a value of about 5% for atmospheric altitudes less than 250 m.

When the boundary condition parameters have been fully set up, the model will be run for analysis with a total of 500 iterations, Fig. 10 shows the fluctuations of the residuals of the quantities participating in the Navier-Stokes equation system based on the RANS method for each iteration. The turbulence model used in this analysis is the $k - \varepsilon$ model. All quantities are stable at iterations of about 250, thereby showing that the model ensures the necessary convergence with 500 iterations.

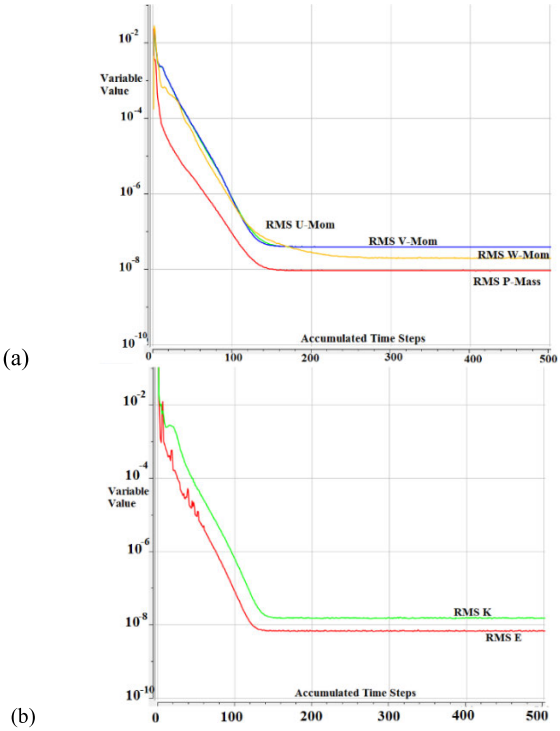

FIGURE 10. Residual fluctuations of the quantities: (a) speed and momentum; (b) k and ε.

When the analysis running is finished, the model is processed to determine the wind speed distribution at the locations along the surface and at the height in 3D space. Fig. 11 shows cross-sections in the direction of the wind

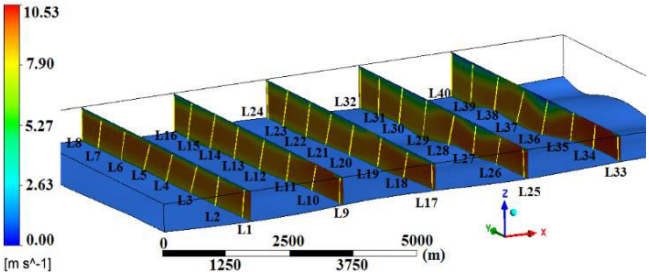

FIGURE 11. Planes perpendicular to the direction of the incoming wind.

and the locations along the cross-sections. Each cross-section plane is 2000 m apart and each location is 1000 m apart.

The wind speeds with height in the range of 200 m above the ground of the straight lines are shown as in Fig. 12. The obtained data shows that the terrain of this area has a gradual increase in height from the southwest to the northeast. The locations in L1 to L8 have a small difference in height, about 50 m. The wind speeds at an altitude of about 100 m above ground level are about 7.5 m/s to 8.0 m/s as shown in Fig. 12(a). Other locations have large elevation differences, the locations in the north have the lowest elevation. On the contrary, the locations in the south have the largest elevation. The elevation difference can be up to nearly 400 m. The wind speeds at an altitude of about 100 m at the northern locations are about 7.5 m/s to 8.0m/s. However, the corresponding wind speeds at the southern locations can reach from 8.0 m/s to 9.5 m/s. In particular, the locations in the northeast have wind speeds up to about 9.0m/s to 10m/s such as L25-L28 and L33-L36 as shown in Fig. 12(d) and Fig. 12(e).

In fact, this area has been installed with Vestas V47/660 wind turbines, the main parameters of which are shown in Table1. This turbine has a tower height of 55 m, a rotor diameter of 47 m, and a capacity of 660 kW when operating at a rated wind speed of 15 m/s. The configuration of the turbines is arranged along 3 hilltops almost parallel to each other as shown in the yellow stars in Fig. 13. The distance between the two nearest turbines is about 100 m in the perpendicular direction and about 2000 m in the direction coinciding with the main wind direction. These locations are very consistent with the calculated results as shown in Fig. 11 and Fig. 12. According to the data in Fig. 12, these locations have average wind speeds of about 8.0 m/s to 10.0 m/s, which is lower than the rated wind speed of Vestas V47/660. This shows that Vestas V47/660 turbines will not be able to achieve their design capacity when operating under actual conditions in the wind farm.

From the satellite data and analysis results, it is clear that the turbine construction areas are reasonable. The turbines are built perpendicular to the main wind direction along the 3 red lines as shown in Fig. 13. All 3 lines run along 3 hillsides, slightly higher than the surrounding area. However, whether the distance between the turbines is optimal or not requires further analysis. The distance between these two horizontal rows is about 2000 m, the distance between 2 turbines close

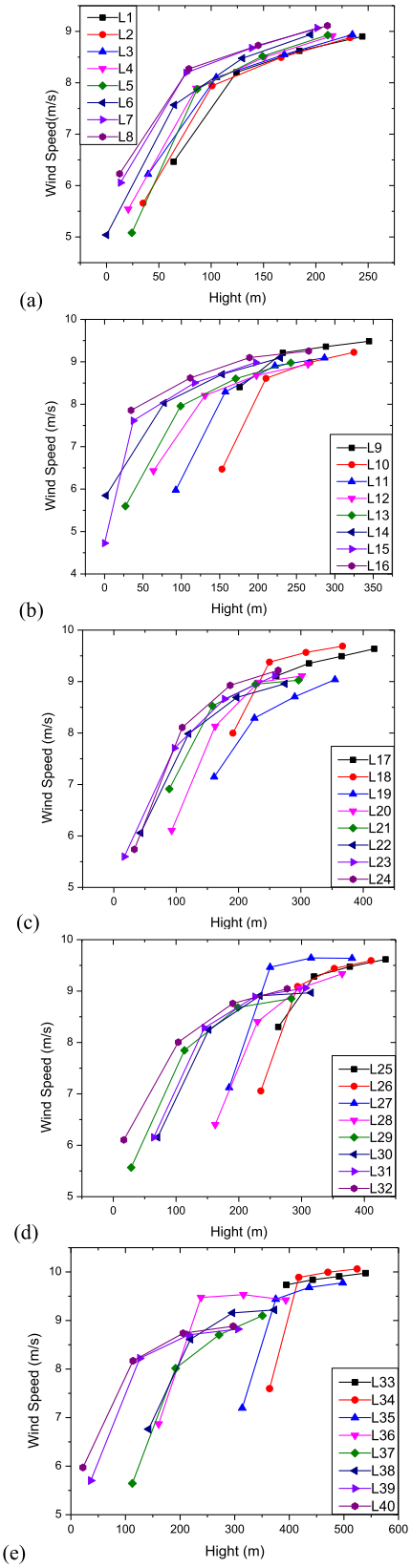

FIGURE 12. Wind speed distributions with height at different locations.

to each other in the horizontal row is about 3Drotor, 100 m, as shown in Fig. 13. According to the data from the [56], [57],

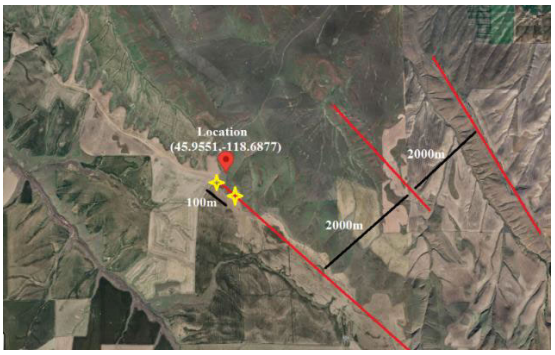

FIGURE 13. Installation area of Vestas V47/660 turbines [63].

the value of the axial reduction factor of the Vestas V47/660 turbine is determined as shown in Fig. 14. If these turbines are operated at wind speeds of 12 m/s or higher, the value of the axial reduction factor will be about 0.1. However, the wind speed according to the analysis is only about 8.0 m/s to 10.0 m/s. Therefore, the value of a is about 0.18. The velocity deficit calculated by the Jensen model as in Eq. (17) and Eq. (18) is 5.6%. This means that the wind speed at the behide turbines in row 2 will be reduced by 5.6% compared to the first row, and row 3 will be reduced by 5.6% compared to the row 2. This difference in wind speed is completely consistent with the operating parameters of the generator [56], [57].

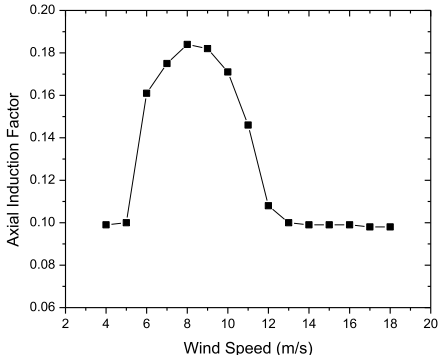

FIGURE 14. Axial reduction factor of Vestas V47/660 turbine with wind speeds.

It is clear that the results obtained from the analytical model are in good agreement with the turbine locations currently installed and operating in this area. However, the analytical results also show that there are some more suitable locations for turbines in this area. The data shown in Fig. 13 shows that the southwest area just in front of the first row of turbines has relatively flat terrain and high wind speeds, but no turbines are installed here. Satellite data shows that this area is under agricultural cultivation. Therefore, no wind turbines are installed here. This shows the benefits of using GIS in this analysis method. In addition to providing topographic features, GIS also clearly shows other infrastructure features such as residential areas, agricultural areas, roads or power transmission systems. Assuming that if this area was exploited, Vestas V47/660 turbines would still be used, then a best configuration of locations can be determined. The configuration of these locations would be in rows across and along the main wind direction in a rectangular shape. The percentage of wind speed loss at the position of the turbine behind the row along the main wind direction is determined as Jensen theory as shown in Fig. 15.

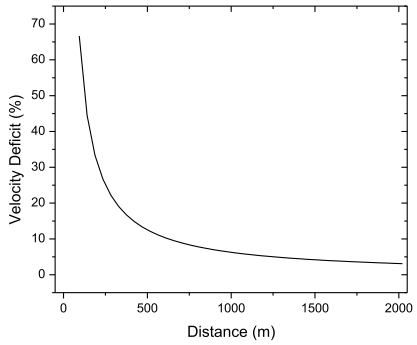

FIGURE 15. Velocity deficit according to the distance between the V47/660 turbines.

From Fig. 15, the velocity deficit value decreases very rapidly with the distance from $2D_{rotor}$ to $10D_{rotor}$. On the contrary, the distance greater than $10D_{rotor}$, the velocity deficit decreases very slowly. If the velocity deficit value is accepted as about 10.0%, then the corresponding distance of the horizontal rows of turbines is 470 m. This area has a wind speed of about 9.0 m/s as shown in Fig. 12(c) and Fig. 12(d). According to the manufacturer's recommendation [56], [57], the minimum distance of the two closest turbines in the main wind direction is $5D_{rotor}$, 235 m. If this recommendation is applied, the velocity deficit at the second turbine will be 48.0% corresponding to a wind speed of 4.68 m/s. At that case, the output power of the rear turbine only reaches 41.79 kW, which is much lower than the design capacity. Obviously, the Vestas V47/660 turbine is not suitable for the wind source characteristics in this area. This area has winds mainly from 8.0 m/s to 10.0 m/s, so turbines with rated wind speeds in this value range will be the most suitable. In addition, the wind speed in this area reaches its best value at a height of about 100 m to 200 m. Therefore, a suitable turbine also needs to have a tower height in this range.

In summary, the results obtained from the analytical model are in high agreement with the actual data. This confirms that the model proposed in this study is highly reliable and can be used to determine the optimal locations for installing wind turbines in any complex terrain conditions.

B. PROPOSED OPTIMAL CONFIGURATION FOR A WIND FARM IN NINH THUAN, VIET NAM

The new method introduced in this study has been verified with an area around the coordinates (45.9551°N, −118.6877°W), the results show high suitability and reliability when compared with the experiment as in Sections III-A–III-B. In this section, the method will be

applied to a wind farm in Ninh Thuan province, Viet Nam and an optimal configuration for the installation location of the turbines will be proposed.

The considered area is around the coordinates (11.4642°N, 109.0049°E) as shown in Fig. 16. The region can be considered as the area with the highest wind speed in Viet Nam.

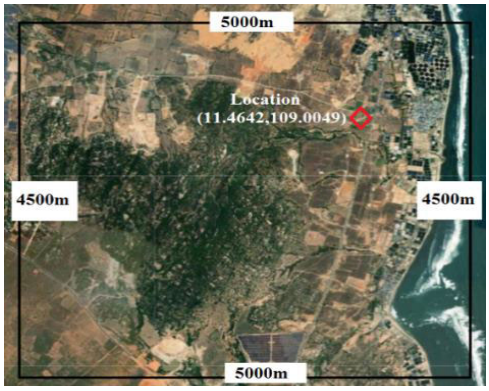

FIGURE 16. Wind farm area around the coordinates (11.4642°N, 109.0049°E) [64].

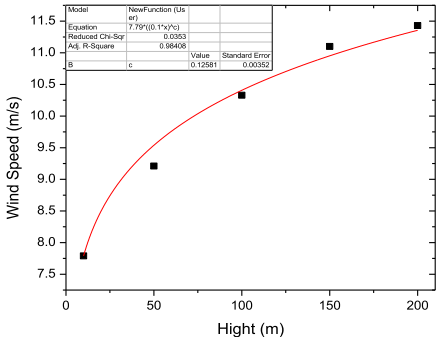

FIGURE 17. Wind speed distribution according to height at inlet plane.

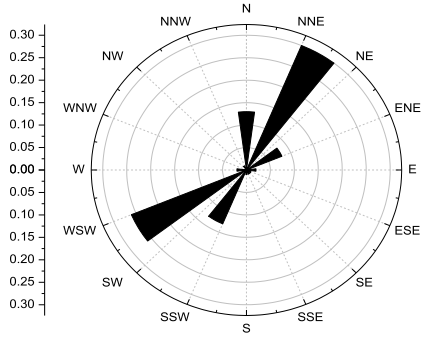

FIGURE 18. Wind direction blowing through this area.

The average wind speed distribution according to height is determined as in Fig. 17 and the wind direction is shown as in Fig. 18. The theoretical fitting function is shown as in Eq. (25):

$$WindSpeed = 7.79 \times \left(\frac{h}{10}\right)^{0.13} \tag{25}$$

The analytical model is built and installed similarly as in Section A. The model has a length of 5000 m, a width of 4500 m, and an air height of 500 m above the lowest point as shown in Fig. 16. The largest grid size is 100 m, the total number of grids is 166495, and the nodes are 38618. The wind speed distribution according to the height at the entrance surface and the incoming wind direction are set according to the parameters in Fig. 17, Fig. 18, and Eq. (25). The main wind direction is determined to be from northeast to southwest. The main wind direction is 60° with the ox axis. This wind direction occurs mainly throughout the year and is almost constant over the planned area. Then, the model will be solved by the RANS method with a total of 500 iterations.

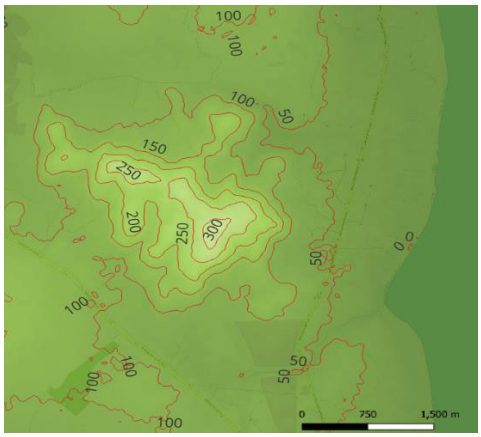

FIGURE 19. Contour lines of terrain elevation in the survey area.

From satellite data as shown in Fig. 16 and contour map in Fig. 19, the mountain top and western areas have steep terrain, about 500 m above sea level. Therefore, it is difficult to install wind turbines here. The northeast area has flat terrain, with convenient roads for transporting and installing wind turbines. Therefore, the wind source in this area will be surveyed in detail. There are 3 cross-sections perpendicular to the east direction are built. Each cross-section is 1000 m apart. Along the cross-section are locations shown in vertical lines, each line is 500 m apart as shown in Fig. 20.

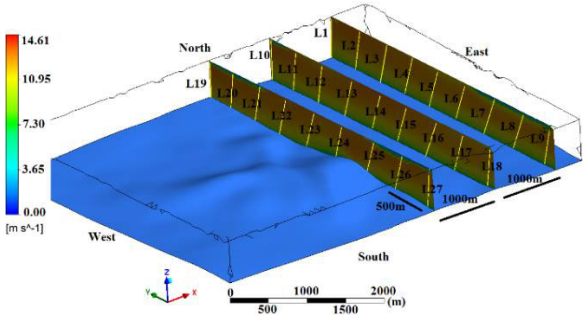

FIGURE 20. Locations surveyed in the model.

The wind speed distributions according to the height of about 200 m above ground level of the locations are shown

in Fig. 21. The results show that the terrain height increases gradually from east to west. The height difference between the sections is about 30 m. The wind speeds at an altitude of about 150 m above the ground also increase gradually from east to west. Fig. 21(a) shows that the wind speed is about 10.5 m/s, Fig. 21(b) shows that the wind speed is about 11.0 m/s, Fig. 21(c) shows that the wind speed is about 11.5 m/s. The wind speed increases because the terrain height increases, the volume of space is reduced according to Bernoulli's law.

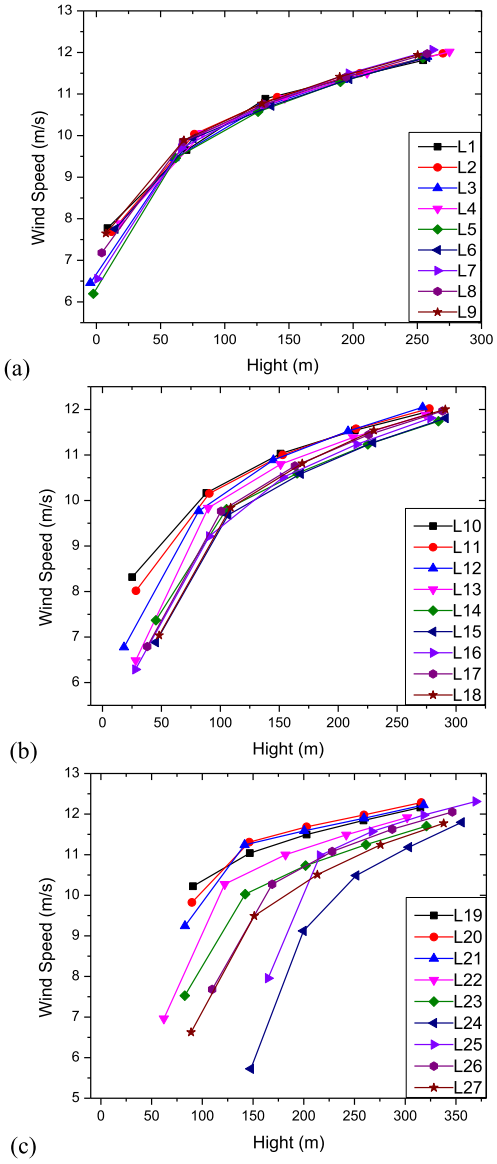

FIGURE 21. Wind speed distributions according to height at locations.

r_{cw} is determined according to the distance (terrain slope) from the first row of turbines at a 100m height above the ground as shown in Fig. 22. These values will be used for terrain-adaptive corrections of wind speed.

Based on the experimental measurements from 2008 to 2010 in this area [65], [66], the values of wind speed and

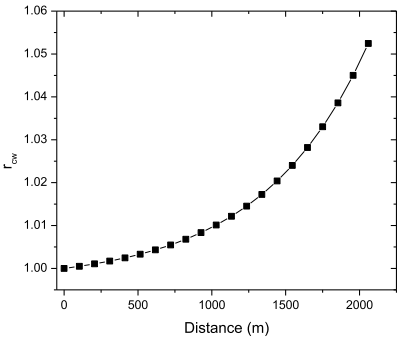

FIGURE 22. r_{cw} changes according to the distance.

wind direction are very similar to the results obtained from the analytical model. The wind speed measurement device has an error of 5%. The Weibull wind speed distribution function in this area according to the main wind direction NNE has parameters W = 2.8 and S = 8.9. The wind speed distribution values according to the Weibull function are shown in Fig. 23 [67].

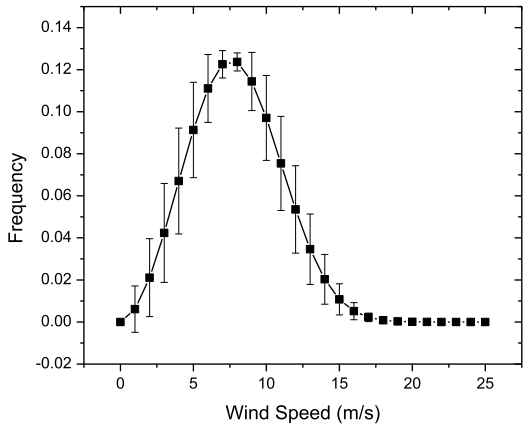

FIGURE 23. Weibull distribution function in the surrounding area.

In fact, this area has been installed with 10 Enercon E103 wind turbines. The locations of these turbine are marked with red stars as shown in Fig. 24. The main technical parameters of E103 are shown in Table 2.

The E103 is a 3-blade horizontal axis turbine, with a rotor diameter of 103 m and a tower height of up to 138 m. The designed capacity is up to 2350 kW when operating at a wind speed of 12 m/s. The dependence of power and power factor of E103 on wind speeds is shown in Fig. 25.

In this study, the area selected for installing the turbines is a flat terrain area as shown in Fig. 19. Therefore, the effects of surface roughness on wind speed and frequency at the hub height of from 98 m to 138 m can be ignored. Eq. (12) and Eq. (14) will be used to determine the AEP values and errors for all cases considered.

From Fig. 24, 10 turbines have been installed scattered in a horizontal row perpendicular to the main wind direction in the

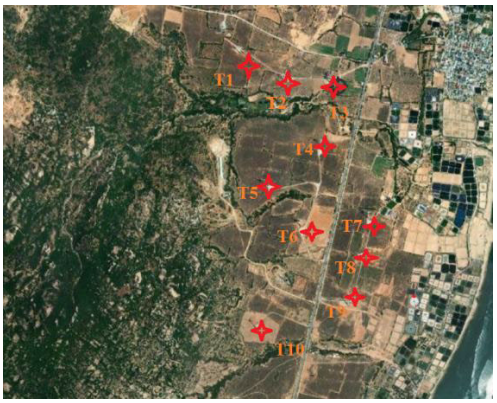

FIGURE 24. Locations of 10 E103 wind turbines [64].

TABLE 2. Some main parameters of ENERCON E103/2350 turbine [68], [69].

Quantity	Value	Quantity	Value
Manufacturer	Enercon	Minimum rotor speed	6 rd/min
Model	E103/2350	Maximum rotor speed	15 rd/min
Rotor diameter	103 m	Cut-in wind speed	2.5 m/s
Number of blades	3	Rated wind speed	12 m/s
Hub height	98 m-138 m	Cut-off wind speed	25 m/s
Power control	Pitch	Rated power	2350 kW

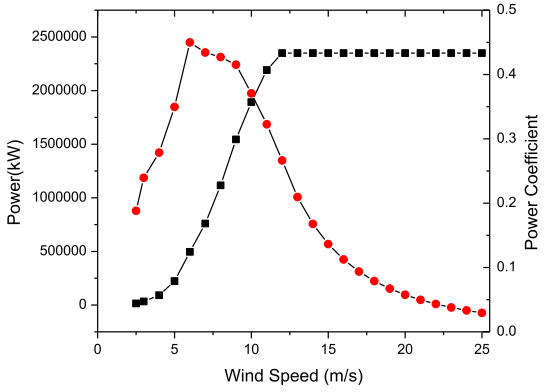

FIGURE 25. Power and power factor of E103 change with wind speed.

eastern area. The distance in the horizontal direction between the turbines is about $3D_{rotor}$, 309 m. The AEP value of the total of these 10 turbines is (99907006.4±25023328.2) kWh. The wake loss determined as in Eq. (16) can be considered as zero in this case, WL = 0%. The AEP value obtained from actual operation announced in 2019 is 100 GWh.

From the satellite image, the turbine positions are not arranged in straight rows, not in any relative shape. This leads to the turbines operating at non-uniform wind speeds, leading to instability in the control of the output electrical parameters. Obviously, the turbines should be installed in horizontal rows perpendicular to the east direction so that all turbines in a row will operate at the same wind speed. The horizontal turbine spacing is about $3D_{rotor}$ as in practice today. The turbine spacing from east to west will depend on the acceptable value of velocity deficit according to Jensen theory. The axial reduction value of E103 with wind speed is shown in Fig. 26. When this turbine operates at wind speeds of about 11m/s or more, the value of a is 0.1.

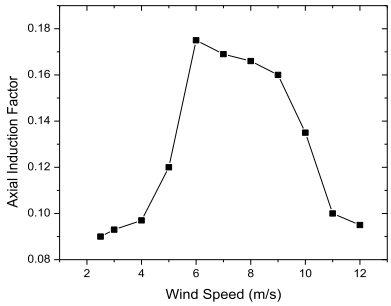

FIGURE 26. Axial reduction factor of E103 with wind speed.

The velocity deficit with distance of the turbines is determined based on Jensen theory for the E103 as shown in Fig. 27. The data shows that the wind velocity deficit decreases sharply with distance from $2D_{rotor}$ to $10D_{rotor}$. From distance greater than $10D_{rotor}$, the wind velocity deficit decreases insignificantly. From here, the optimal distance for installing the turbines is 1030 m. At this distance, the velocity deficit is about 11.8%. This value is generally accepted in the actual operation of wind farms.

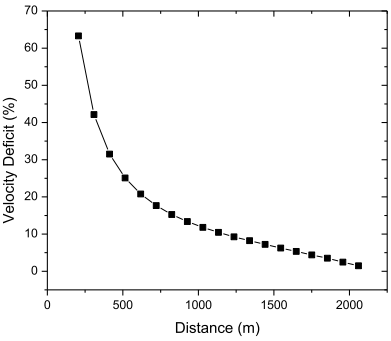

FIGURE 27. Wind velocity deficit with distance of E103 turbines.

According to Fig. 16 and Fig. 19, the flat area from the coast to the foot of the mountain is about 2500 m. When excluding the residential area, the area where wind turbines can be installed is about 2000 m wide and 4000 m long. The configurations that can be installed are as follows: If the distance between the rows of turbines is $3D_{rotor}$, 6 rows can be installed; if the distance is $4D_{rotor}$, 4 rows can be installed; if the distance is $5D_{rotor}$ to $6D_{rotor}$, 3 rows can be installed; if the distance is $7D_{rotor}$ - $10D_{rotor}$, 2.5 rows can be installed; if the distance is from $11D_{rotor}$ to $19D_{rotor}$, 2 rows can be installed;

TABLE 3. Some main results of these configurations.

Configuration	WL (%)	AEP (GWh/year)	LCOE ($/MWh)
Real Configuration	0	99.9 ± 25.0	67.1 ± 16.8
3D	78.8	152.8 ± 41.8	315.7 ± 86.3
4D	61.5	184.6 ± 51.9	174.3 ± 49.0
6D	35.8	230.8 ± 64.9	104.5 ± 29.4
10D	15.8	252.3 ± 67.4	79.7 ± 21.3
19D	1.5	236.1 ± 59.8	68.1 ± 17.2
20D	0	119.9 ± 30.0	67.1 ± 16.8

if the distance is over $20D_{rotor}$, only 1 row can be installed. These configurations are specifically calculated as shown in Table 3, Fig. 28 and Fig. 29.

- Configuration 1: Installing with a row spacing of $3D_{rotor}$, the distance between the two closest turbines in each row is $3D_{rotor}$, the total number of turbines is 72. Then the wind speed at each row of turbines behind will be reduced by 42.2% according to the values in Fig. 27. This causes the 4^{th} row turbines to have wind speeds below the operating value, only the first 3 rows can operate. The total AEP is (152778722.7 ± 41745155.8) kWh and WL is 78.8%.

- Configuration 2: Installing with a row spacing of $4D_{rotor}$, the distance between the two closest turbines in each row is $3D_{rotor}$, the total number of turbines is 48. Then the wind speed at each row of turbines behind will be reduced by 31.7% respectively according to the values in Fig. 27. The total AEP is (184596510.4 ± 51939780.0) kWh and WL is 61.5%.

- Configuration 3: Installing with a row spacing of $6D_{rotor}$, the distance between the two nearest turbines in each row is $3D_{rotor}$, the total number of turbines is 36. Then the wind speed at each row of turbines behind will be reduced by 21.1% respectively as shown in Fig. 27. The total AEP is (230843859.7 ± 64878160.2) kWh and WL is 35.8%.

- Configuration 4: Installing with a row spacing of $10D_{rotor}$, the distance between the two closest turbines in each row is $3D_{rotor}$, the total number of turbines is 30. Then the wind speed at each row of turbines behind will be reduced by 11.8% respectively according to the values in Fig. 27. The total AEP is (252349323.7 ± 67449682.6) kWh and WL is 15.8%.

- Configuration 5: Installing with a row spacing of $19D_{rotor}$, the distance between the two nearest turbines in each row is $3D_{rotor}$, the total number of turbines is 24. Then the wind speed at each row of turbines behind will be reduced by 2.5% respectively as shown in Fig. 27. The total AEP is (236118269.7 ± 59766995.9) kWh and WL is 1.5%.

- Configuration 6: Installing with a row spacing of $20D_{rotor}$, the distance between the two closest turbines in each row is $3D_{rotor}$, the total number of turbines is 12. Then the wind speed at each row of turbines behind will be reduced by 6.3% respectively as shown in Fig. 27. The total AEP is (119888407.7 ± 30027993.8) kWh and there is no wake loss due to the front turbine in this case.

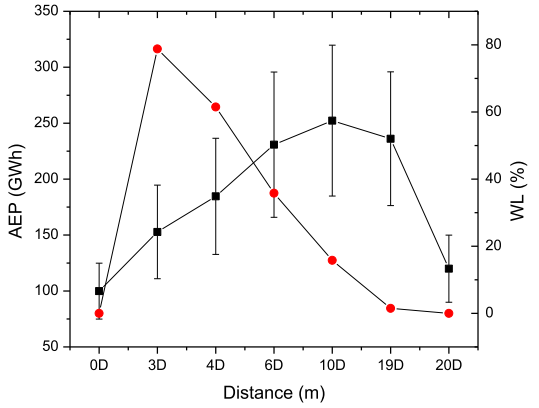

FIGURE 28. AEP and wake loss change according to distance between the E103 turbines.

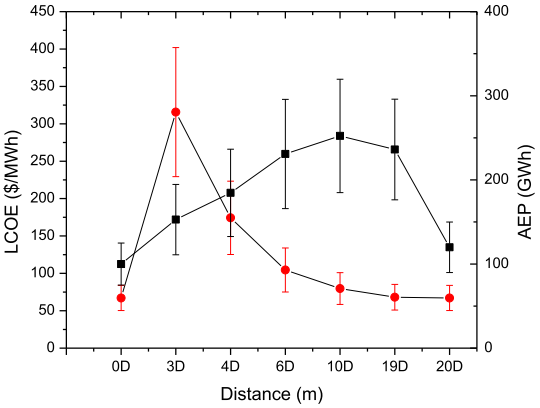

FIGURE 29. Optimal configuration for installing the E103 turbines.

Comparing the results obtained from 1 real configuration and 6 different assumed configurations as shown in Fig. 28, configuration 4 with a row spacing of $10D_{rotor}$ gives the largest AEP and a very small WL value of only 15.8%. To confirm the suitability of the configuration in practice, an LCOE assessment is performed. According to the [70], [71], the LCOE of a 2.6 MW turbine is determined as Eq. (26):

$$LCOE = \frac{CapEx + \sum_{i=1}^{T} OpEx_i \,(1+r)^{-i}}{\sum_{i=1}^{T} AEP_i \,(1+r)^{-i}} \tag{26}$$

In which: LCOE is the levelized cost of energy, $/MWh; T is the operating time of the farm, 20 years; r is the discount rate, 14.6%; CapEx is the project capital cost, 1436 $/kW; OpEx is the operating cost, 43 $/kW/year; AEP is the annual energy output, MWh/year.

The LCOE values of the cases are shown in the Table 3 and Fig. 29.

FIGURE 30. Optimal configuration for installing the E103 turbines [64].

It is clear that the LCOE values of the turbine spacing cases from 10D onwards change very little. The LCOE value is about 79.7 $/MWh for the 10D configuration and 67.1 $/MWh for the existing configuration. The 10D configuration is the most optimal configuration for the E103 turbines installed at this wind farm. The third row of this configuration has half of it going through the mountainside, so it is not possible to install turbines here. Fig. 30 illustrates the installation configuration of E103 turbines in the survey area with a spacing of $10D_{rotor}$. The installation locations of the turbines are shown as yellow stars.

If the E103 turbines are installed at the locations marked with stars in Fig. 30, the output power of the turbines will be more uniform. This helps with control and output electricity quality. In addition, the total number of turbines that can be installed in this area is 30, which is 3 times larger than the actual number. The annual electricity production of the optimal configuration can be about 2.5 times larger than the current configuration.

When comparing the existing configuration and the 20D configuration in case of 10 turbines. Configuration 20D has the turbines arranged in a horizontal row along the coast. All turbines are at the same terrain height, leading to more uniformity in installation, operation, maintenance and annual power output. In contrast, the current configuration has a zigzag distribution. This causes natural instabilities when the wind blows from the east, causing certain difficulties in the operation and grid connection. This once again shows the superiority that the method proposed in this study can bring. This method can solve strategic problems, bringing the highest efficiency to investors in the wind power sector globally.

In summary, some E103 turbines have been built in this area to exploit wind energy. However, the installation locations and the number of existing E103 turbines have not achieved the best efficiency. The optimal location determination method proposed in this paper has determined an optimal configuration. This configuration increases the total annual electricity production of the wind farm by 2.5 times compared to the present. This once again confirms the benefits that this method can bring to wind farms. This method will contribute to promoting the efficient exploitation of wind energy in countries, contributing to increasing the contribution rate of wind power to sustainable human development.

IV. CONCLUSION

The paper has presented the method for determining the optimal number and location of wind turbines in complex terrain conditions and the area has been determined. This method is intuitive, taking into account many factors depending on the actual terrain such as surface roughness, terrain height, roads, residential areas, and LCOE. This method does not require high computer systems, and the calculation time is fast. This can be considered an advantage of this method when compared with other methods such as LES and WRF or artificial intelligence algorithms.

The data on wind speed and wind direction at heights below 200 m are referenced from the WorldBank data source. The comparison results with the actual measured data from the CBWES project show that the difference is very small, less than 1%. This is a reliable and important data source in the planning of wind farm projects. However, to obtain more reliable results, it is still necessary to measure wind data at one location in the area to determine the exact parameters of the Weibull wind frequency distribution function. From there, the AEP value will be predicted more accurately.

The results obtained from applying this method to a wind farm in Ninh Thuan province, Viet Nam show its superiority and the ability to bring great benefits to wind farm projects. Thereby, this method can be used as a reliable source of assessment for planning the construction of wind farms in the world. In future studies, this method will be combined with additional infrastructure databases including roads and power grids to be more complete in the optimization problem of wind farms. The goal is to maximize the AEP and minimize the LCOE for onshore wind farm projects.

REFERENCES

[1] S.-P. Moon, S.-Y. Kim, R. Labios, and Y.-B. Yoon, "Determining wind farm locations, allocation of wind farm capacity, and sizing of energy storage for 17 GW new wind power capacity in Korea," in *Proc. IEEE Power Energy Soc. Gen. Meeting (PESGM)*, Jul. 2016, pp. 1–5.

[2] M. James, M. Jon, and R. Anthony, *Wind Energy Explained: Theory, Design and Application*. Hoboken, NJ, USA: Wiley, 2009.

[3] M. Lydia, S. S. Kumar, A. I. Selvakumar, and G. E. P. Kumar, "Wind resource estimation using wind speed and power curve models," *Renew. Energy*, vol. 83, pp. 425–434, Nov. 2015.

[4] S. Qureshi, F. Shaikh, L. Kumar, F. Ali, M. Awais, and A. E. Gürel, "Short-term forecasting of wind power generation using artificial intelligence," *Environ. Challenges*, vol. 11, Apr. 2023, Art. no. 100722.

[5] V. Simankov, P. Buchatskiy, S. Teploukhov, S. Onishchenko, A. Kazak, and P. Chetyrbok, "Review of estimating and predicting models of the wind energy amount," *Energies*, vol. 16, no. 16, p. 5926, Aug. 2023.

[6] D. Song, X. Tan, Q. Huang, L. Wang, M. Dong, J. Yang, and S. Evgeny, "Review of AI-based wind prediction within recent three years: 2021–2023," *Energies*, vol. 17, no. 6, p. 1270, Mar. 2024.

[7] M. B. Ashraf, M. A. Siddiqui, and M. U. Yousuf, "Autoregressive integrated moving average (ARIMA) modeling for wind resource assessment," *Int. J. Energy Water Resources*, vol. 8, no. 2, pp. 187–198, Jun. 2024.

[8] T. Khan, I. Ahmad, Y. Wang, M. Salam, A. Shahzadi, and M. Batool, "Comparison approach for wind resource assessment to determine the most precise approach," *Energy Environ.*, vol. 35, no. 3, pp. 1315–1338, May 2024.

[9] T. Sudarshan, C. Srinivasulu, H. P. Thethi, V. Bhutani, P. Subhashini, and G. Ramesh, "Optimizing wind turbine placement for enhanced energy production using modified genetic algorithm," in *Proc. 7th Int. Conf. Contemp. Comput. Informat. (IC3I)*, Greater Noida, India, Sep. 2024, pp. 638–642.

[10] M. S. Gomez, J. K. Lundquist, J. D. Mirocha, R. S. Arthur, D. Munoz-Esparza, and R. Robey, "Can LiDARs assess wind plant blockage in simple terrain? A WRF-LES study," *J. Renew. Sustain. Energy*, vol. 14, no. 6, Nov. 2022, Art. no. 063303.

[11] W. Hu, Q. Yang, Z. Yuan, and F. Yang, "Wind farm layout optimization in complex terrain based on CFD and IGA-PSO," *Energy*, vol. 288, Feb. 2024, Art. no. 129745.

[12] J. Sanz Rodrigo, R. A. Chávez Arroyo, P. Moriarty, M. Churchfield, B. Kosović, P.-E. Réthoré, K. S. Hansen, A. N. Hahmann, J. D. Mirocha, and D. Rife, "Mesoscale to microscale wind farm flow modeling and evaluation," *WIREs Energy Environ.*, vol. 6, no. 2, p. e214, Mar. 2017.

[13] NCAR. *Weather Research & Forecasting Model (WRF)*. Accessed: Feb. 1, 2025. [Online]. Available: https://www.mmm.ucar.edu/models/wrf

[14] S. J. Andersen, S.-P. Breton, B. Witha, S. Ivanell, and J. N. Sørensen, "Global trends in the performance of large wind farms based on high-fidelity simulations," *Wind Energy Sci.*, vol. 5, no. 4, pp. 1689–1703, Dec. 2020.

[15] R. K. Rai, L. K. Berg, B. Kosović, J. D. Mirocha, M. S. Pekour, and W. J. Shaw, "Comparison of measured and numerically simulated turbulence statistics in a convective boundary layer over complex terrain," *Boundary-Layer Meteorol.*, vol. 163, no. 1, pp. 69–89, Apr. 2017.

[16] L. K. Berg, M. Pekour, and D. Nelson, "Description of the Columbia basin wind energy study (CBWES)," U.S. Dept. Energy, Pacific Northwest Nat. Lab. Richland, Washington, DC, USA, Tech. Rep. PNNL-22036, 2012.

[17] B. Yang, L. K. Berg, Y. Qian, C. Wang, Z. Hou, Y. Liu, H. H. Shin, S. Hong, and M. Pekour, "Parametric and structural sensitivities of turbine-height wind speeds in the boundary layer parameterizations in the weather research and forecasting model," *J. Geophys. Res., Atmos.*, vol. 124, no. 12, pp. 5951–5969, Jun. 2019.

[18] L. Niyomtham, C. Lertsathittanakorn, J. Waewsak, and Y. Gagnon, "Mesoscale/microscale and CFD modeling for wind resource assessment: Application to the Andaman coast of southern Thailand," *Energies*, vol. 15, no. 9, p. 3025, Apr. 2022.

[19] V. Santhanagopalan, L. Y. Al-Hamidi, S. Letizia, L. Zhan, and G. V. Iungo, "Profitability optimization of a wind power plant performed through parabolic RANS simulations and an economic model," in *Proc. Wind Energy Symp., AIAA SciTech Forum*, Jan. 2018, pp. 1–8.

[20] G. Gualtieri, "Comparative analysis and improvement of grid-based wind farm layout optimization," *Energy Convers. Manage.*, vol. 208, Mar. 2020, Art. no. 112593.

[21] D. Bensason, E. Simley, O. Roberts, P. Fleming, M. Debnath, J. King, C. Bay, and R. Mudafort, "Evaluation of the potential for wake steering for U.S. land-based wind power plants," *J. Renew. Sustain. Energy*, vol. 13, no. 3, May 2021, Art. no. 033303.

[22] A. P. J. Stanley, O. Roberts, J. King, and C. J. Bay, "Objective and algorithm considerations when optimizing the number and placement of turbines in a wind power plant," *Wind Energy Sci.*, vol. 6, no. 5, pp. 1143–1167, Sep. 2021.

[23] S. Pranupa, A. T. Sriram, and R. S. Nagaraja, "A review of wind farm layout optimization techniques for optimal placement of wind turbines," *Int. J. Renew. Energy Res.*, vol. 13, no. 2, pp. 1–10, 2023.

[24] A. S. Benabadji, K. Rahmoun, F. A. Bahar, A. Dahani, A. Martinez, and G. Iglesias, "Geospatial LCOE analysis for floating offshore wind energy in SW Mediterranean Sea," *Renew. Energy*, vol. 245, Jun. 2025, Art. no. 122797.

[25] R. J. Barthelmie, G. C. Larsen, S. T. Frandsen, L. Folkerts, K. Rados, S. C. Pryor, B. Lange, and G. Schepers, "Comparison of wake model simulations with offshore wind turbine wake profiles measured by sodar," *J. Atmos. Ocean. Technol.*, vol. 23, no. 7, pp. 888–901, Jul. 2006.

[26] T. Göçmen, P. Van Der Laan, P.-E. Réthoré, A. Pena Diaz, G. C. Larsen, and S. Ott, "Wind turbine wake models developed at the technical University of Denmark: A review," *Renew. Sustain. Energy Rev.*, vol. 60, pp. 752–769, Jul. 2016.

[27] S. Kumar, R. K. Saket, D. K. Dheer, P. Sanjeevikumar, J. B. Holm-Nielsen, and F. Blaabjerg, "Layout optimisation algorithms and reliability assessment of wind farm for microgrid integration: A comprehensive review," *IET Renew. Power Gener.*, vol. 15, no. 10, pp. 2063–2084, Jul. 2021.

[28] A. P. J. Stanley, O. Roberts, A. Lopez, T. Williams, and A. Barker, "Turbine scale and siting considerations in wind plant layout optimization and implications for capacity density," *Energy Rep.*, vol. 8, pp. 3507–3525, Nov. 2022.

[29] Z. Liu, W. Wang, Y. Wang, and T. Ishihara, "Large eddy simulations of slope effects on flow fields over isolated hills and ridges," *J. Wind Eng. Ind. Aerodyn.*, vol. 201, Jun. 2020, Art. no. 104178.

[30] J. Singh and J. M. Alam, "Large-eddy simulation of utility-scale wind farm sited over complex terrain," *Energies*, vol. 16, no. 16, p. 5941, Aug. 2023.

[31] Y. Li, Z. Li, Z. Zhou, and X. Yang, "Large-eddy simulation of wind turbine wakes in forest terrain," *Sustainability*, vol. 15, no. 6, p. 5139, Mar. 2023.

[32] N. N. Kethavath and N. S. Ghaisas, "Effect of an abrupt rough-to-smooth surface roughness transition on wind farm wakes: An LES and analytical modeling study," *J. Renew. Sustain. Energy*, vol. 16, no. 3, May 2024, Art. no. 033302.

[33] C. Pan, S. Wen, M. Zhu, J. Ma, and C. Hou, "DC collector system layout optimization for offshore wind farm with SPP topology," *IEEE Trans. Sustain. Energy*, vol. 16, no. 2, pp. 1269–1282, Apr. 2025.

[34] D. V. Thin, N. H. Duc, L. Q. Sang, and D. V. Binh, "Study to evaluate the effect of terrain surface on performance of a wind farm in Ninh Thuan province, Vietnam," in *Proc. E3S Web Conf.*, 2023, p. 1038.

[35] Q. Wu, Y. Wang, H. Sun, H. Lin, and Z. Zhao, "A system coupled GIS and CFD for atmospheric pollution dispersion simulation in urban blocks," *Atmosphere*, vol. 14, no. 5, p. 832, May 2023.

[36] Y. Back, P. Kumar, P. M. Bach, W. Rauch, and M. Kleidorfer, "Integrating CFD-GIS modelling to refine urban heat and thermal comfort assessment," *Sci. Total Environ.*, vol. 858, Feb. 2023, Art. no. 159729.

[37] G. V. Iungo, V. Santhanagopalan, U. Ciri, F. Viola, L. Zhan, M. A. Rotea, and S. Leonardi, "Parabolic RANS solver for low-computational-cost simulations of wind turbine wakes," *Wind Energy*, vol. 21, no. 3, pp. 184–197, Dec. 2017.

[38] P. I. Muiruri, O. S. Motsamai, and R. Ndeda, "A comparative study of RANS-based turbulence models for an upscale wind turbine blade," *Social Netw. Appl. Sci.*, vol. 1, no. 3, p. 237, Mar. 2019.

[39] Whiffle. *Wind Resource Assessment and Yield Modelling: Comparing 4 Models—LES, Meso-Scale, CFD-RANS and Engineering*. Accessed: Feb. 1, 2025. [Online]. Available: https://whiffle.nl/blog/wind-resource-assessment-model-comparison/

[40] Ministry of Industry and Trade of the Socialist Republic of Vietnam. *Approval of Adjusted Power Plan VIII*. Accessed: Feb. 1, 2025. [Online]. Available: https://moit.gov.vn/tin-tuc/phat-trien-nang-luong/chinh-thuc-phe-duyet-quy-hoach-dien-viii-dieu-chinh.html

[41] A. Peña, P.-E. Réthoré, and O. Rathmann, "Modeling large offshore wind farms under different atmospheric stability regimes with the park wake model," *Renew. Energy*, vol. 70, pp. 164–171, Oct. 2014.

[42] L. Q. Sang, T. Phengpom, D. V. Thin, N. H. Duc, L. T. T. Hang, C. T. T. Huyen, N. T. T. Huong, and Q. T. Tran, "A method to design an efficient airfoil for small wind turbines in low wind speed conditions using XFLR5 and CFD simulations," *Energies*, vol. 17, no. 16, p. 4113, Aug. 2024.

[43] Z. Shu and M. Jesson, "Estimation of Weibull parameters for wind energy analysis across the U.K.," *J. Renew. Sustain. Energy*, vol. 13, no. 2, Mar. 2021, Art. no. 023303.

[44] F. González-Longatt, P. Wall, and V. Terzija, "Wake effect in wind farm performance: Steady-state and dynamic behavior," *Renew. Energy*, vol. 39, no. 1, pp. 329–338, Mar. 2012.

[45] R. Jia, M. Ge, Z. Zhang, X. Li, and B. Du, "A numerical simulation framework for wakes downstream of large wind farms based on equivalent roughness model," *Energy*, vol. 307, Oct. 2024, Art. no. 132600.

[46] P. Díaz-Cuevas, "GIS-based methodology for evaluating the wind-energy potential of territories: A case study from Andalusia (Spain)," *Energies*, vol. 11, no. 10, p. 2789, Oct. 2018.

[47] F. M. I. Flora, N. Donatien, R. Tchinda, and O. Hamandjoda, "Selection wind farm sites based on GIS using a Boolean method: Evaluation of the case of Cameroon," *J. Power Energy Eng.*, vol. 9, no. 1, pp. 1–24, 2021.

[48] A. Demir, A. E. Dinçer, C. Çiftçi, S. Gülçimen, N. Uzal, and K. Yılmaz, "Wind farm site selection using GIS-based multicriteria analysis with life cycle assessment integration," *Earth Sci. Informat.*, vol. 17, no. 2, pp. 1591–1608, Apr. 2024.

[49] A. Salih, A. A. Hassaballa, and M. A. Eltawil, "Integrating spatial data and multi-criteria analysis for wind farm suitability mapping in eastern Saudi Arabia," *Energy*, vol. 301, Aug. 2024, Art. no. 131623.
[50] GitHub Inc. *BlenderGIS*. Accessed: Feb. 1, 2025. [Online]. Available: https://github.com/domlysz/BlenderGIS
[51] T. Koblitz, A. Bechmann, J. Berg, A. Sogachev, N. Sørensen, and P.-E. Réthoré, "Atmospheric stability and complex terrain: Comparing measurements and CFD," *J. Phys., Conf. Ser.*, vol. 555, Dec. 2014, Art. no. 012060.
[52] Ansys Inc. *What is Computational Fluid Dynamics*. Accessed: Feb. 1, 2025. [Online]. Available: https://www.ansys.com/simulation-topics/what-is-computational-fluid-dynamics
[53] Ansys Inc. *Ansys Innovation Courses: Calculating Turbulent Intensity*. Accessed: Feb. 1, 2025. [Online]. Available: https://innovationspace.ansys.com/courses/courses/topics-in-turbulence-modeling-using-ansys-fluent/lessons/calculating-turbulent-intensity
[54] A. Sogachev and O. Panferov, "Modification of two-equation models to account for plant drag," *Boundary-Layer Meteorol.*, vol. 121, no. 2, pp. 229–266, Oct. 2006.
[55] A. Sogachev, "A note on two-equation closure modelling of canopy flow," *Boundary-Layer Meteorol.*, vol. 130, no. 3, pp. 423–435, Mar. 2009.
[56] The Wind Power. *Vestas V47/660*. Accessed: Jul. 26, 2024. [Online]. Available: https://en.wind-turbine-models.com/turbines/13-vestas-v47
[57] *General Specification 660 KW Variable Slip Wind Turbines, V47–660kW; V47–660/200 KW, Item No.: 943111.R4*, Vestas Wind Systems A/S, Aarhus, Denmark, 2024.
[58] H.-G. Kim, Y.-H. Kang, and J.-Y. Kim, "Evaluation of wind resource potential in mountainous region considering morphometric terrain characteristics," *Wind Eng.*, vol. 41, no. 2, pp. 114–123, Apr. 2017.
[59] DTU. *Global Wind Atlas*. Accessed: Feb. 1, 2025. [Online]. Available: https://globalwindatlas.info/en/?fbclid=IwY2xjawE6Z3tleHRuA2FlbQIxMAABHVcf4aRhS3JFWbHxMvk-7MFb8A_QHHO_a2HXXu23Gw-vO_ooDi1g7buW8Q_aem_ZwQ-_D52ApSHjfUvS-5mJQ
[60] D. Solyali, M. Altunç, S. Tolun, and Z. Aslan, "Wind resource assessment of northern Cyprus," *Renew. Sustain. Energy Rev.*, vol. 55, pp. 180–187, Mar. 2016.
[61] B. Yang, Y. Qian, L. K. Berg, P.-L. Ma, S. Wharton, V. Bulaevskaya, H. Yan, Z. Hou, and W. J. Shaw, "Sensitivity of turbine-height wind speeds to parameters in planetary boundary-layer and surface-layer schemes in the weather research and forecasting model," *Boundary-Layer Meteorol.*, vol. 162, no. 1, pp. 117–142, Jan. 2017.
[62] L. Bianco, P. Muradyan, I. Djalalova, J. M. Wilczak, J. B. Olson, J. S. Kenyon, R. Kotamarthi, K. Lantz, C. N. Long, and D. D. Turner, "Comparison of observations and predictions of daytime planetary-boundary-layer heights and surface meteorological variables in the Columbia river gorge and basin during the second wind forecast improvement project," *Boundary-Layer Meteorol.*, vol. 182, no. 1, pp. 147–172, Jan. 2022.
[63] Google. *Googlemaps*. Accessed: Feb. 1, 2025. [Online]. Available: https://www.google.com/maps/place/45%C2%B057'18.4%22N+118%C2%B041'15.7%22W/45.9507093,-118.6867442,739m/data=!3m1!1e3!4m4!3m3!8m2!3d45.9551!4d-118.6877?hl=vi-VN&entry=ttu&g_ep=EgoyMDI0MDgyMy4wIKXMDSoASAFQAw%3D%3D
[64] Google. *Googlemaps*. Accessed: Feb. 1, 2025. [Online]. Available: https://www.google.com/maps/11.4574465,108.9992077,2821m/data=!3m1!1e3?entry=ttu&g_ep=EgoyMDI0MDkwNC4wIKXMDSoASAFQAw%3D%3D
[65] K. A. Huynh, "Assessment of wind energy potential based on data in phan Rang–Ninh Thuan published by the world bank," Power Eng. Consulting Joint Stock Co., Hanoi, Vietnam, Tech. Rep., Apr. 2016.
[66] AWS Truepower llc. *MOIT_Vietnam_Wind_Atlas*. Accessed: Feb. 1, 2025. [Online]. Available: https://www.esmap.org/sites/esmap.org/files/MOIT_Vietnam_Wind_Atlas_Report_18Mar2011.pdf
[67] MedCalc Software Ltd. *Weibull Distribution Functions*. Accessed: Feb. 1, 2025. [Online]. Available: https://www.medcalc.org/manual/weibull-distribution-functions.php
[68] The Wind Power. *Enercon E103/2350*. Accessed: Feb. 1, 2025. [Online]. Available: https://www.thewindpower.net/turbine_en_1107_enercon_e103-2350.php
[69] Viuredelaire. *Aerogenerator Enercon E-103 EP2*. Accessed: Feb. 1, 2025. [Online]. Available: https://www.viuredelaire.cat/index.php?md=articles&id=13543&lg=eng
[70] T. Stehly, P. Beiter, and P. Duffy, "Cost of wind energy review," Nat. Renew. Energy Lab., Denver, CO, USA, Tech. Rep. NREL/TP-5000-81209, 2020.
[71] B. Thomas, X. Costoya, M. deCastro, D. Carvalho, and M. Gómez-Gesteira, "Wake effect impact on the levelized cost of energy in large floating offshore wind farms: A case of study in the Northwest of the Iberian peninsula," *Energy*, vol. 304, Sep. 2024, Art. no. 132159.

DINH VAN THIN received the B.S. and M.S. degrees in atomic and nuclear physics from Hanoi University of Science-Vietnam National University, Vietnam, in 2012 and 2015, respectively. Currently, he is pursuing the Ph.D. degree in energy engineering major with Electric Power University.

He has been a Lecturer at the Faculty of New Energy, Electric Power University, since 2013. His main research interests include research and evaluation of optimal designs for power plants, such as nuclear power, wind power, solar power, wave/tidal power, and biomass power.

LE QUANG SANG received the Ph.D. degree in system engineering from Mie University, Japan, in 2018. He joint postdoctoral program in China Academy Science, in 2019. From 2007 to 2024, he was a Researcher with the Institute of Science and Technology for Energy and Environment, Vietnam Academy of Science and Technology. He also a Lecturer with the Faculty of Energy Engineering, School of Electrical and Electronics Engineering, Hanoi University of Industry. He focused on wind power technology and renewable energy. He is the author more than 40 articles and conferences. He is the manager and main participant many projects related to renewable energy in Vietnam. His research interests include wind technology, CFD simulation, and renewable energy.

NGUYEN HUU DUC (Member, IEEE) received the B.S. degree (Hons.) in electrical power systems from Hanoi University of Science and Technology, Vietnam, in 2006, and the Dr.-Ing. degree from the Technical University of Berlin (TU), in 2014.

From 2009 to 2014, he was a Ph.D. Student and a Researcher at TU Berlin. He is currently an Associate Professor specialized in renewable energy and the Deputy Dean of the Energy Technology Faculty and used to be the Head of the Renewable Energy Department, Electric Power University. He is also the Chair of the Innovations for Sustainable and Renewable Energy Sources and Systems Laboratory (ISRESS Lab). His research focuses on the areas of renewable energy sources modeling, renewable energy integration, distributed control systems, energy storage, electric vehicles, and policies on renewable energy development in Vietnam. He has realized several projects, such as ac/dc next generation networks, virtual power plants, green buildings, PV integrations, small wind turbines, electric vehicles, and charging stations based on PV. He has been (co-)author of two books, and has published more than 80 publications in journals and conference proceedings. He has supervised around 20 master's/Ph.D. theses. He is a Technical Member of TCVN for renewable sources and electric vehicles.